Contrasting response of hydrological cycle over land and ocean to a changing CO2 pathway

Yeh, S.-W. ORCID: https://orcid.org/0000-0003-4549-1686, Song, S.-Y. ORCID: https://orcid.org/0000-0002-9447-1158, Allan, R. P. ORCID: https://orcid.org/0000-0003-0264-9447, An, S.-I. ORCID: https://orcid.org/0000-0002-0003-429X and Shin, J. ORCID: https://orcid.org/0000-0002-3199-7646 (2021) Contrasting response of hydrological cycle over land and ocean to a changing CO2 pathway. npj Climate and Atmospheric Science, 4 (1). 53. ISSN 2397-3722 doi: 10.1038/s41612-021-00206-6 Available at https://centaur.reading.ac.uk/101019/

ARTICLE   OPEN

Check for updates

Contrasting response of hydrological cycle over land and ocean to a changing CO_2 pathway

Sang-Wook Yeh [1]✉, Se-Yong Song [1], Richard P. Allan [2], Soon-Il An [3] and Jongsoo Shin [3]

The hydrological cycle has a significant impact on human activities and ecosystems, so understanding its mechanisms with respect to a changing climate is essential. In particular, a more detailed understanding of hydrological cycle response to transient climate change is required for successful adaptation and mitigation policies. In this study, we exploit large ensemble model experiments using the Community Earth System Model version 1.2.2 (CESM1) in which CO_2 concentrations increase steadily and then decrease along the same path. Our results show that precipitation changes in the CO_2 increasing and decreasing phases are nearly symmetrical over land but asymmetric over oceans. After CO_2 concentrations peak, the ocean continues to uptake heat from the atmosphere, which is a key process leading the hydrological cycle's contrasting response over land and ocean. The symmetrical hydrological cycle response over land involves a complex interplay between rapid responses to CO_2 and slower responses to ensuing warming. Therefore, the surface energy constraints lead to the contrasting hydrological response over land and ocean to CO_2 forcing that needs to be verified and considered in climate change mitigation and adaption actions.

INTRODUCTION

The global hydrological cycle's responses to rising temperatures driven by increasing greenhouse gas concentration significantly impact human activities and Earth's ecosystems[1–8]. Extreme rainfall events are becoming more intense[9–11], raising serious concerns for human vulnerability[12]. Furthermore, damaging floods and drought frequency are projected to increase[13,14]. The magnitude and rate of changes for regional hydrological events directly impact infrastructure, agriculture, and health[15–17].

Previous studies examined precipitation changes in warmer climates by analyzing Coupled Model Intercomparison Projection Phase 5 (CMIP5) climate models. These climate change simulations are characterized by a wet-get-wetter/dry-get-drier pattern[18–20] or a warmer-get-wetter pattern[21,22] over the oceans. Water vapor content at typical lower troposphere temperatures is constrained to increase by no more than 7% K^{-1} [18], which is the limit set by the Clausius–Clapeyron equation for saturation vapor pressure. Changes in the rate of global precipitation and evaporation response to warming differ significantly from water vapor content changes[2,3,18]. Most CMIP5 models predict hydrological sensitivity around 1–3% K^{-1}[17]. The discrepancy between water vapor content changes and hydrological sensitivity can be explained by net radiative surface and atmospheric energy balance constraints that limit latent heat flux increases driven by a warmer climate[2], an important consequence of which is atmospheric circulation slowdown[18,23]. Although this perspective explains the hydrological cycle changes reasonably well, the scientific community requires more detailed understanding of hydrological cycle sensitivity to transient climate change[24].

Studies investigating hydrological sensitivity to atmospheric CO_2 removal are of importance, because they provide climate mitigation plans and emission reduction replacements[25–29]. Some climate mitigation studies assume a linear relationship between temperature and precipitation with respect to increasing or decreasing atmospheric CO_2 concentrations[30,31]. The global hydrological cycle, however, demonstrates known hysteresis behavior and this has important implications for atmospheric emission reductions and carbon capture[32]. Furthermore, it is important to differentiate the hydrological cycle's response over oceans and land in a changing CO_2 pathway. In this study, we focus on understanding the physical processes associated with hydrological sensitivities to idealized transient CO_2 increases and removal over land and oceans, respectively, which has never been attempted in a previous study. We used 28 climate simulation ensemble sets along with a present-day climate simulation (PD simulation) using the standard Community Earth System Model version 1.2.2 (CESM1) (see "Methods").

A standard metric for assessing the sensitivity of climate to radiative forcing is the Equilibrium Climate Sensitivity, which quantifies the global average surface temperature change resulting from a doubling of CO_2 concentration from a pre-industrial period after the climate system equilibrates. However, in the present study we are interested in examining the physical processes determining hydrological sensitivity and how this determines global water cycle changes over time, thereby providing information relevant for ongoing climate mitigation and adaptation plans from the present climate condition.

Unless stated otherwise in the text, all analyses use the annual mean of the 28-member ensemble with the deviation obtained by subtracting the PD simulation climatology from the ensemble mean.

RESULTS

Changes in precipitation and temperature to CO_2 forcing

Figure 1a displays changes in CO_2 concentration including an increase (ramp-up) and decrease (ramp-down) period. The CO_2 concentration during the stabilization period is identical to that in

[1]Department of Marine Science and Convergent Engineering, Hanyang University, Ansan, South Korea. [2]Department of Meteorology and National Centre for Earth Observation, University of Reading, Reading, UK. [3]Department of Atmospheric Sciences/Irreversible Climate Change Research Center, Yonsei University, Seoul, South Korea. ✉email: swyeh@hanyang.ac.kr
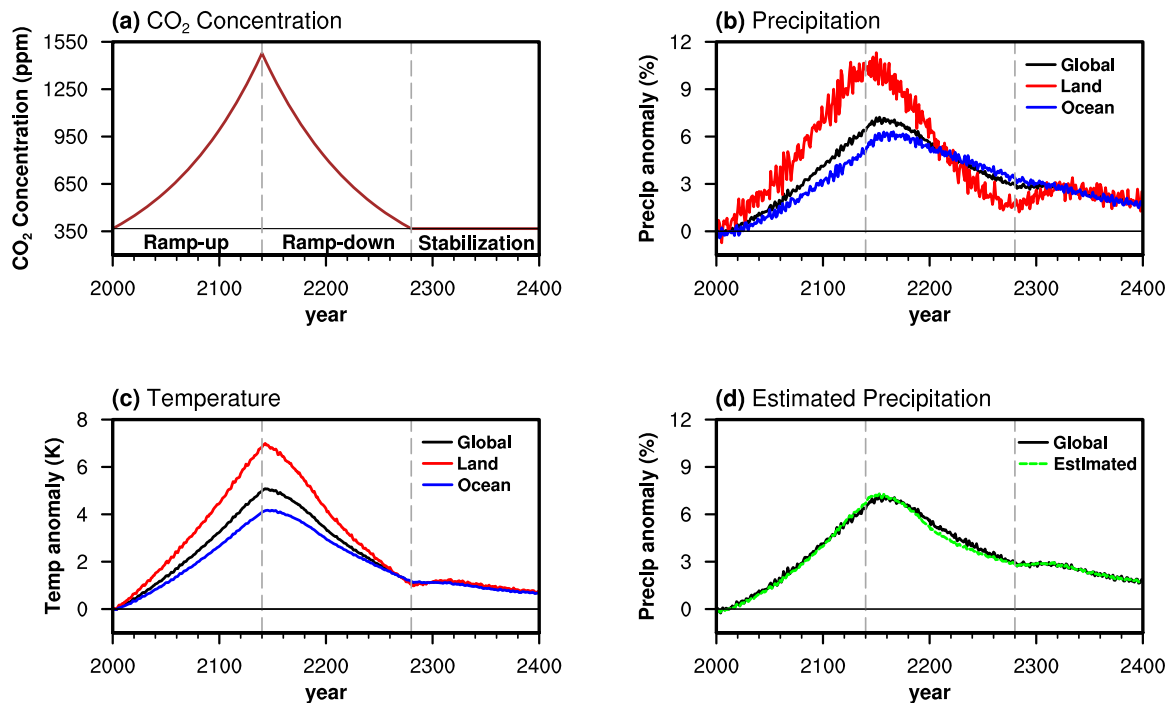
Fig. 1 Mean precipitation and temperature changes for a changing CO$_2$ pathway. a Changes in CO$_2$ concentration for an increase (ramp-up) period, a decrease (ramp-down) period, and a stabilization period. **b** Changes in global, land, and ocean mean precipitation from the ramp-up period to the stabilization period compared to the PD simulation. **c** Same as **b**, except for surface temperature anomaly. **d** Changes in global mean precipitation from the ramp-up period to the stabilization period compared to the PD simulation (black) and the estimated global mean precipitation (green) using a simple conceptual model (see "Methods").

the PD simulation. Global mean precipitation increases during the CO$_2$ ramp-up period and continues to increase for almost two decades after peak CO$_2$ concentration (Fig. 1a, b).

Although the changes in global mean precipitation are almost identical to the changes in ocean precipitation, land precipitation changes are almost symmetric in a changing CO$_2$ pathway (Fig. 1b). During the stabilization period, neither the global mean precipitation nor ocean and land precipitation returns to the present climate conditions, as the adjustment back to the PD simulation is likely to be slow after 280 continuous years of excess heating, much of which is stored in the deep ocean.

The precipitation is 2% higher than the present climate conditions after 120 years of stabilization in both land and ocean (Fig. 1b). This indicates that the precipitation responses to a changing CO$_2$ pathway are not symmetric[33,34]. Similar behavior is seen for global mean surface temperature (Fig. 1c). The evolution of the temperature is largely corresponding to changes in CO$_2$, suggesting a linear response, although its peak is delayed some years because of the heat capacity of the ocean, and the rate of temperature decrease in the ramp-down period is smaller in magnitude than the rate of increase in the ramp-up period[27,35]. We demonstrate that the hydrological cycle hysteresis is different for oceans and land (Fig. 1b). Ocean and land temperature changes in response to changing CO$_2$ are similar, except for their magnitudes (Fig. 1c), which is mainly due to a large heat capacity in the ocean. Consequently, there is an almost linear relationship between precipitation and temperature change for land in response to a changing CO$_2$ concentration (Supplementary Fig. 1 and see also Fig. 2b), which contrasts with the asymmetric relationship of precipitation and temperature change over the ocean (Supplementary Fig. 2 and see also Fig. 2c). We discuss the detailed physical processes later.

Global mean precipitation response to CO$_2$ concentration changes is a combination of an initial fast (days to weeks) atmospheric adjustment to radiative forcing and a slower

response to surface temperature change[34]. This has previously been explained by considering the atmospheric and surface energy budgets[36], and it can be illustrated using a simple conceptual model (see "Methods" for details). It is found that the estimated global mean precipitation response based on the atmospheric and surface energy budgets is well matched with the global mean precipitation response simulated in CESM1 (Fig. 1d). This implies that the precipitation response (ΔP) is explained by the fast (ΔP_{fast}) and slow (ΔP_{slow}) precipitation response to temperature change in a CESM1. It is noteworthy that Δ indicates the deviation from PD simulation climatology. Therefore, we obtain the following equation

$$\Delta P = \kappa \Delta T = \Delta P_{fast} + \Delta P_{slow} = \Delta P_{fast} + \alpha \Delta T \qquad (1)$$

Here, κ is an apparent hydrological sensitivity, which represents the total change of precipitation per degree surface warming compared to PD climate. α is a hydrological sensitivity, which is defined by the increase in precipitation solely due to a given change in temperature and it can be estimated from the stabilization phase where $\Delta P_{fast} = 0$. This equation can be applied to global, ocean, or land, respectively.

An apparent global hydrological sensitivity (κ_{global}) is 1.35% K^{-1} for the CO$_2$ ramp-up period and it is significantly reduced to 1.09% K^{-1} for the CO$_2$ ramp-down period (Supplementary Fig. 3a, b, d). However, κ_{global} increases to 2.54% K^{-1} during the stabilization period (Supplementary Fig. 3c, e and Table 1). This is consistent with energetic arguments in previous studies showing that global precipitation response to temperature change is larger when CO$_2$ concentrations are constant than when they change over time[34,37]. It is noteworthy that the CO$_2$ changes suppress the apparent global hydrological sensitivity below 2.54% K^{-1} equally in ramp-up and ramp-down. However, the delayed temperature response, which is mostly due to the ocean heat capacity, tends to suppress this response more in the ramp-down period (Fig. 2a and Table 1). Therefore, removing
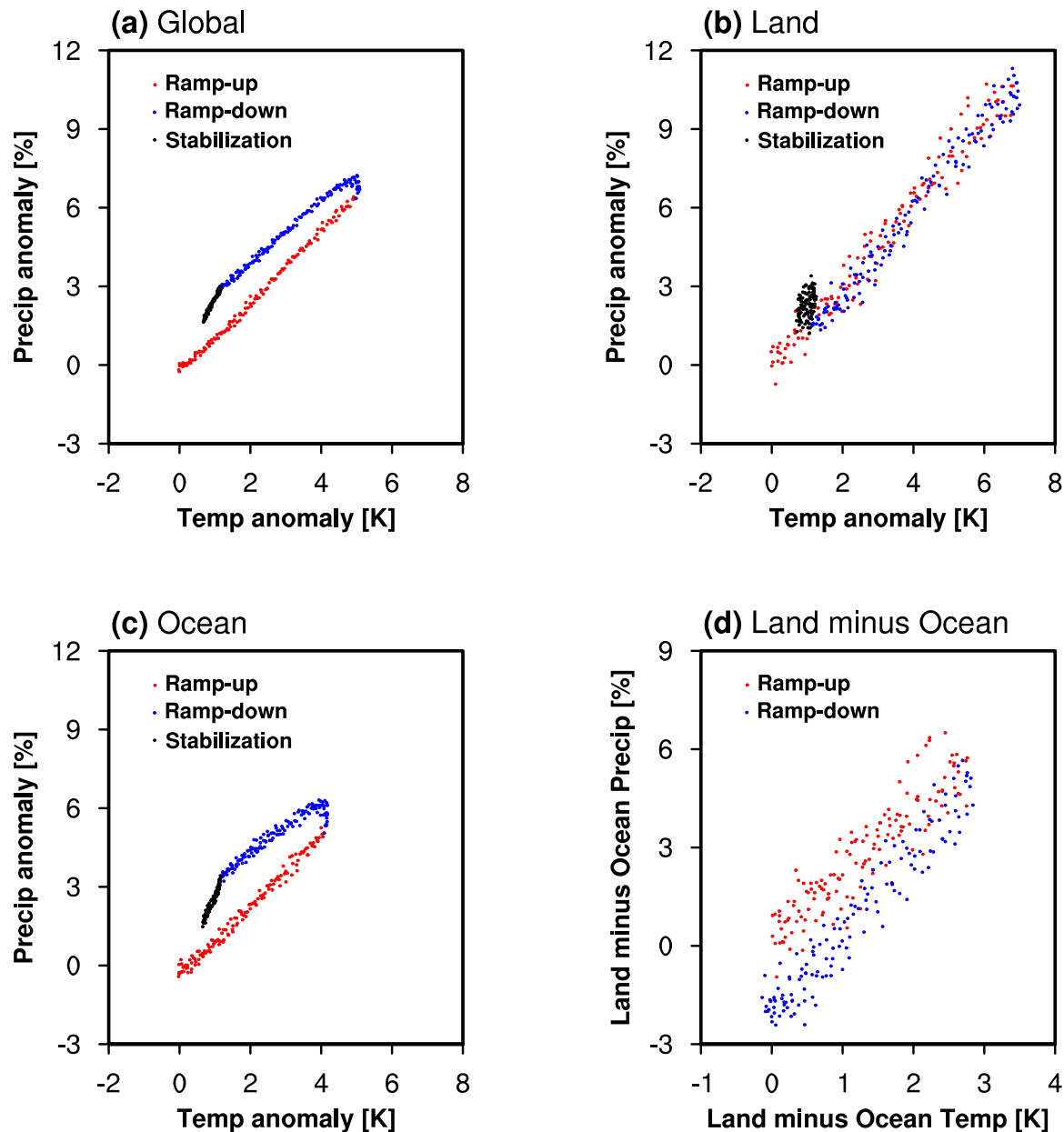
Fig. 2 Precipitation and temperature relationship changes during CO₂ ramp-up, ramp-down, and stabilization periods. a The percentage change of global mean precipitation and the global mean surface temperature anomaly during CO_2 ramp-up, ramp-down, and stabilization periods. **b–d** Same as **a**, except they are over land, ocean, and land minus ocean, respectively. Each dot represents the annual mean anomaly obtained by subtracting the PD simulation climatology from the ensemble mean. The percentage anomaly is defined as the difference between the ensemble mean and PD simulation divided by PD simulation.

Table 1. Summary of hydrological sensitivity and apparent hydrological sensitivity in a CESM1.

	α Hydrological sensitivity	κ Apparent hydrological sensitivity
Global	2.54% K⁻¹	1.35% K⁻¹ (ramp-up ↑)
		1.09% K⁻¹ (ramp-down↓)
Land	1.21% K⁻¹	1.57% K⁻¹ (ramp-up ↑)
		1.61% K⁻¹ (ramp-down↓)
Ocean	3.09% K⁻¹	1.32% K⁻¹ (ramp-up ↑)
		0.86% K⁻¹ (ramp-down↓)

atmospheric CO_2 may cause a significant climate mitigation side effect by reducing the magnitude of precipitation to the ensuing cooling due to the mitigation and then abruptly increasing hydrological cycle sensitivity once the CO_2 concentration stabilizes. This indicates a need for careful climate mitigation and emission reduction planning.

Contrasting hydrological sensitivity over land and ocean

Subsequently, we calculate the precipitation response to atmospheric adjustment, to radiative forcing over oceans and land,
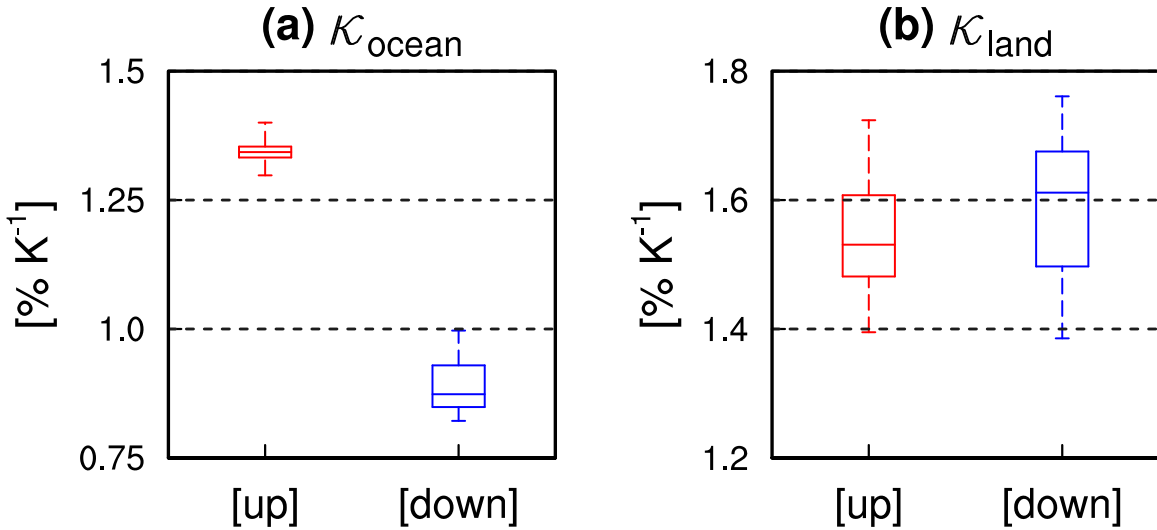
(a) $\mathcal{K}_{\text{ocean}}$

(b) $\mathcal{K}_{\text{land}}$

Fig. 3 Ocean and land hydrological sensitivity for each ensemble member. a Box-and-whisker diagram of apparent ocean hydrological sensitivity (κ_{ocean}) during CO_2 ramp-up and ramp-down periods. The box plot and whiskers represent quartiles with median and total range, respectively, in each period. **b** Same as **a**, except apparent land hydrological sensitivity (κ_{land}).

respectively, following Eq. (1).

$$\Delta P_{\text{ocean fast}\uparrow} = (\kappa_{\text{ocean}\uparrow} - a_{\text{ocean}})\Delta T_{\text{ocean}} \quad (2)$$

$$\Delta P_{\text{ocean fast}\downarrow} = (\kappa_{\text{ocean}\downarrow} - a_{\text{ocean}})\Delta T_{\text{ocean}} \quad (3)$$

$$\Delta P_{\text{land fast}} = (\kappa_{\text{land}} - a_{\text{land}})\Delta T_{\text{land}}, \quad (4)$$

($\uparrow$: ramp − up period, $\downarrow$: ramp − down period)

a_{ocean}, a_{land}, κ_{land}, $\kappa_{\text{ocean}\uparrow}$, and $\kappa_{\text{ocean}\downarrow}$ values are summarized with those in the globe in Table 1.

Here, the characteristics of the apparent hydrological sensitivity over the ocean (κ_{ocean}) and land (κ_{land}) are different during the ramp-up and ramp-down periods (Fig. 2b, c and Table 1). Although κ_{ocean} is not the same for the CO_2 ramp-up ($\kappa_{\text{ocean}\uparrow} = 1.32\% \, K^{-1}$) and ramp-down ($\kappa_{\text{ocean}\downarrow} = 0.86\% \, K^{-1}$) periods (Figs. 2c and 3a), κ_{land} (1.59% K^{-1}) is nearly identical over land for both periods (Figs. 2b and 3b) (see also "Methods"). This implies that CO_2 changes equally influence the apparent hydrological sensitivity over land in ramp-up and ramp-down, which is in contrast to oceans.

On the other hand, land precipitation changes from rising temperatures, which are influenced by tropospheric temperature adjustments to CO_2 radiative forcing, are increased by 0.38% K^{-1} (κ_{land} (1.59% K^{-1}) − a_{land} (1.21% K^{-1})). That is, the CO_2 radiative forcing drives an additional increase in precipitation as land temperatures rise. This phenomenon could be related to land–ocean temperature contrast (Fig. 2d), i.e., warmer land than ocean may lead to more convergence over land, resulting in an additional increase in precipitation. In contrast, ocean precipitation changes from CO_2 radiative forcing are suppressed by 1.77% K^{-1} during the CO_2 ramp-up period ($\kappa_{\text{ocean}\uparrow}$ (1.32% K^{-1}) − a_{ocean} (3.09% K^{-1})) and 2.23% K^{-1} during the CO_2 ramp-down period ($\kappa_{\text{ocean}\downarrow}$ (0.86% K^{-1}) − a_{ocean} (3.09% K^{-1})), implying that the CO_2 radiative forcing drives an additional decrease in precipitation as ocean temperatures rise. These results indicate that CO_2 radiative forcing leads to a contrast in the fast precipitation response between land and oceans[38,39]. Furthermore, the CO_2 radiative forcing tends to suppress the precipitation changes over the ocean more in the ramp-down period than in the ramp-up period, which is due to the delayed ocean temperature response in the ramp-down period (Fig. 2d).

We used 28 climate simulation ensemble sets along with the PD simulation; therefore, a deviation in each ensemble from the

Table 2. Summary of SDs of apparent hydrological sensitivity (κ) in 28 CESM1 ensemble members.

	Ocean	Land
Ramp-up↑	0.023% K^{-1}	0.080% K^{-1}
Ramp-down↓	0.052% K^{-1}	0.102% K^{-1}

ensemble mean could be due to internal climate variability[40,41]. We calculate the standard deviation (SD) of apparent ocean and land hydrological sensitivity in 28 climate simulation ensemble sets, respectively (Fig. 3 and see also Table 2). It is found that the SD of $\kappa_{\text{ocean}\downarrow}$ is significantly larger than that of $\kappa_{\text{ocean}\uparrow}$, implying that the role of internal climate variability on apparent ocean hydrological sensitivity is large during the CO_2 ramp-down period compared to that during the CO_2 ramp-up period. A similar phenomenon is also observed in apparent hydrological sensitivity over land (Table 2). However, the increase of SD over land from the ramp-up to the ramp-down period is smaller than the ocean. These results indicate that the role of internal climate variability on apparent hydrological sensitivity over the ocean and land is changing from the CO_2 ramp-up to the ramp-down period and its contribution differs over the ocean and land, respectively.

Contrasting precipitation changes over land and ocean constrained by energy budget

As precipitation changes are constrained by atmospheric and surface energy budgets[2,34,42,43], we also examine the land and ocean global surface energy budgets.

$$\Delta Q_L = \Delta R_{\text{Lnet}} + \Delta R_{\text{Snet}} - \Delta Q_S : \text{Land} \quad (5)$$

$$\Delta Q_L = \Delta R_{\text{Lnet}} + \Delta R_{\text{Snet}} - \Delta Q_S + \Delta R_{\text{TOA}} : \text{Ocean} \quad (6)$$

Here, Q_L is latent heat flux from the surface, R_{Lnet} is net longwave radiation, R_{Snet} is net shortwave radiation, and Q_S is the upward sensible heat flux. R_{TOA} is the net radiation at the top of the atmosphere, which balances with ocean heat uptake (i.e., -R_{TOA})[37] and we assume land heat uptake is negligible. The right-hand side of Eq. (5) can be seen in Fig. 4a. Changes in net longwave radiation (ΔR_{Lnet}) and net shortwave radiation (ΔR_{Snet}) are compensated by changes in sensible heat flux (ΔQ_S).

Land

(a) Longwave, Shortwave, Sensible

(b) Latent, Radiative cooling

(c) Latent & Precipitation

Ocean

(d) Longwave, Shortwave, Sensible

(e) Latent, Ocean heat uptake, Radiative cooling
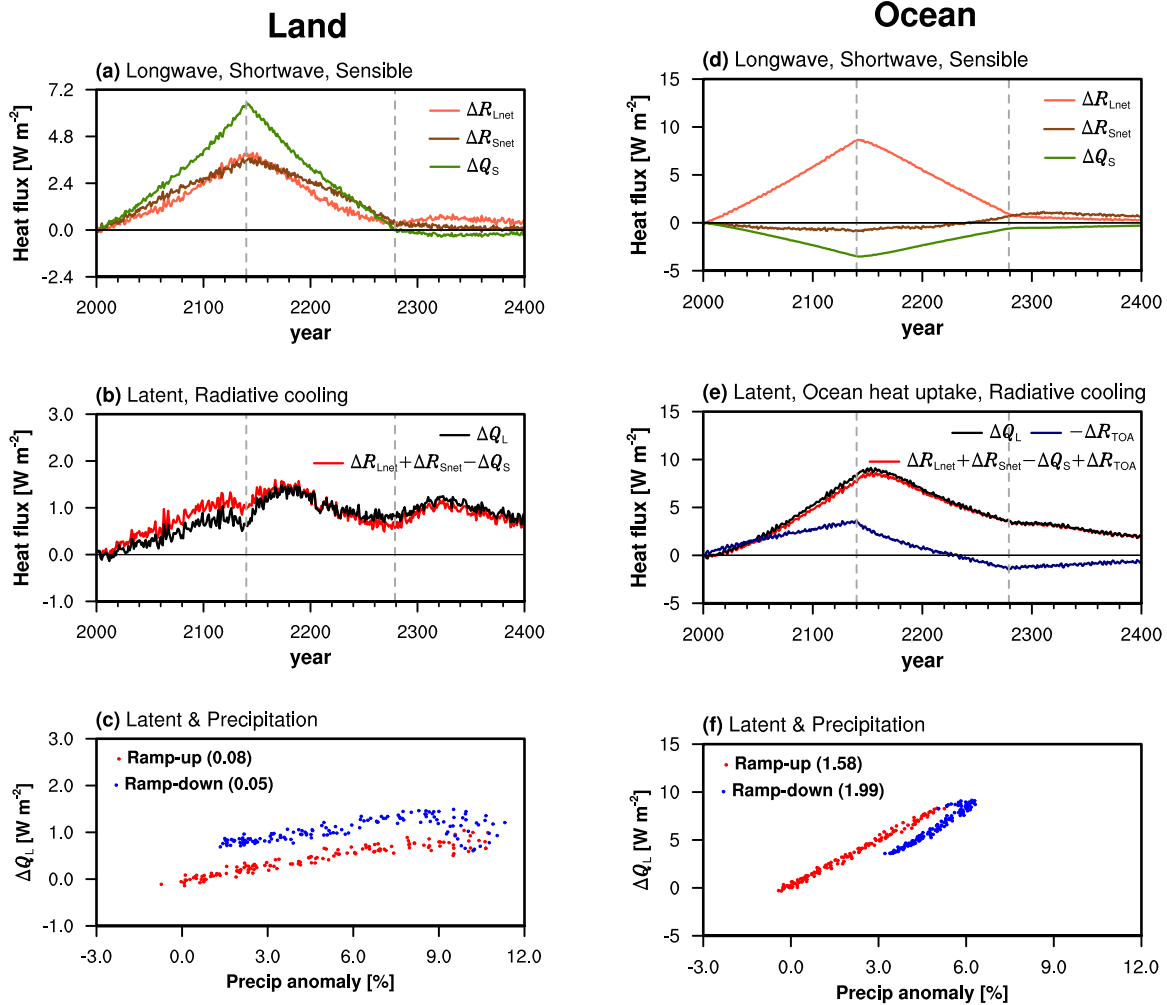
(f) Latent & Precipitation

Fig. 4 Changes in land and ocean surface energy budgets and precipitation changes. Changes in land **a** ΔR_{Lnet}, ΔR_{Snet}, and ΔQ_S, **b** ΔQ_L and $(\Delta R_{Lnet} + \Delta R_{Snet} - \Delta Q_S)$ during CO_2 ramp-up, ramp-down, and stabilization periods. **c** Relationship between ΔQ_L and precipitation percentage change in land during CO_2 ramp-up and ramp-down periods. Changes in ocean **d** ΔR_{Lnet}, ΔR_{Snet}, and ΔQ_S, **e** ΔQ_L ($\Delta R_{Lnet} + \Delta R_{Snet} - \Delta Q_S + \Delta R_{TOA}$) and $-\Delta R_{TOA}$ during CO_2 ramp-up, ramp-down, and stabilization periods. **f** Relationship between ΔQ_L and precipitation percentage change in ocean during CO_2 ramp-up and ramp-down periods. Δ indicates the deviation from the PD climatology simulation. Bracket values represent linear regression coefficients between ΔQ_L and the precipitation percentage change, which are statistically significant at a 99% confidence level.

Consequently, changes in latent heat flux (ΔQ_L) balance with ΔR_{Lnet}, ΔR_{Snet}, and ΔQ_S (Fig. 4b). As ΔQ_L changes are tied to land precipitation changes (Fig. 4c), we conclude that the almost symmetric land precipitation response (see also Supplementary Fig. 1) is mainly constrained by the symmetric change in surface energy terms ΔR_{Lnet}, ΔR_{Snet}, and ΔQ_S (Fig. 4a). This implies that the overall land precipitation response is strongly constrained by the fast response to CO_2 radiative forcing's tropospheric temperature adjustment. Over land, the tropospheric temperature adjustments during CO_2 ramp-up and ramp-down decreases atmospheric stability and increases convection compared to that during the present climate condition[2,36,44], leading to increased precipitation[45]. This is also explained by an increased land–ocean temperature contrast with warming (see also Fig. 2d), which drives decreased atmospheric stability and dominates over the direct atmospheric and surface heating effect of elevated CO_2 over land. The land–ocean warming contrast relating to differing thermal capacities of land and ocean but also contrasting surface feedbacks explains the increased hydrological sensitivity over land[46] (i.e., 0.38% K^{-1}).

Figure 4d, e display the right-hand side of Eq. (6) (ΔR_{Lnet}, ΔR_{Snet}, ΔQ_S, and ΔR_{TOA}) for oceans, respectively. Figure 4e also shows ΔQ_L

changes are identical to the four surface energy terms combined and it is also tied to ocean precipitation changes (Fig. 4f). Therefore, the ocean precipitation response is also constrained by changes in surface energy terms ΔR_{Lnet}, ΔR_{Snet}, ΔQ_S, and ΔR_{TOA}, consistent with land (Fig. 4b, e). In contrast to land, however, changes in sensible heat flux (ΔQ_S) are negative (i.e., downward) over the ocean during both CO_2 ramp-up and ramp-down periods (Fig. 4d). This is because land warms more than ocean; therefore, the sea surface temperature is changing less than the atmosphere above it (Supplementary Fig. 4). This is also associated with the suppression of ($\kappa_{ocean} - \alpha_{ocean}$) during both periods (Eqs. (2) and (3)), which is explained by the direct atmospheric heating by CO_2 radiative forcing, while the land–ocean warming contrast partly offset this effect.

In addition, changes in both ocean heat uptake ($-\Delta R_{TOA}$) (Fig. 4e) and net shortwave radiation (ΔR_{Snet}) (Fig. 4d) explain the asymmetric precipitation response to oceanic temperature changes (Fig. 4f). Unlike the symmetric ΔQ_S and ΔR_{Lnet} changes, both ΔR_{Snet} and ΔR_{TOA} changes are asymmetric. ΔR_{Snet} changes its sign in the latter stages of the CO_2 ramp-down period and the ocean receives more net shortwave radiation during the CO_2 stabilization period (Fig. 4d). After peak atmospheric CO_2

concentration, on the other hand, $-\Delta R_{TOA}$ slowly decreases and changes sign in the middle of the CO_2 ramp-down period (Fig. 4e). These characteristics contribute to the asymmetric precipitation response over the oceans. In particular, the oceans absorb heat until the middle of the CO_2 ramp-down period despite the CO_2 concentration decrease. In addition, the oceans continue to release heat despite a fixed CO_2 concentration during the stabilization period. We speculate that this may contribute to increased ΔR_{Snet} during and after the latter stages of the CO_2 ramp-down (Fig. 4d). There is a possibility that ocean heat release into atmosphere may reduce the amount of low-level clouds over the oceans during the stabilization period (Supplementary Fig. 5) through enhanced low-level turbulence in boundary layer[47]. This may act to increase net shortwave radiation at the surface. However, we cannot exclude the possibility that the extra heat released to the atmosphere may destabilize it, enhance convection, leading to more cloudiness, and hence reduced shortwave radiation at the surface. It is therefore valuable to further analyze the detailed mechanisms, although it is beyond the scope of the present study.

Meanwhile, there is a contrast in both "slopes" and "direction" in the relationship between ΔQ_L and precipitation percentage change over land and the ocean during CO_2 ramp-up and ramp-down periods, respectively (Fig. 4c, f). This implies that there is different moisture divergence from over the ocean and convergence over land during CO_2 ramp-up and ramp-down periods. The low slopes over land (Fig. 4c) reflects weaker dependence of precipitation on evaporation than that over the ocean. Therefore, the enhanced precipitation must be due more to enhanced moisture convergence from the oceans (e.g., stronger monsoons) than to local evaporation. However, the increased latent heat loss through surface evaporation over land during the CO_2 ramp-down period (Fig. 4c) does not reflect warmer or wetter land during this period, because temperature is relatively symmetric between the CO_2 ramp-up and ramp-down periods (see Fig. 1b). Therefore, the increased latent heat loss over land could be explained by a smaller contribution of moisture import from the oceans to land precipitation during the CO_2 ramp-down period. A smaller contribution of moisture convergence to precipitation over land during the CO_2 ramp-down period then requires more surface evaporation over land for the same precipitation anomaly. On the other hand, the larger slopes in the relationship between ΔQ_L and precipitation percentage change over the ocean than land (Fig. 4c, f) indicates that precipitation over the ocean must be closely proportional to surface evaporation compared to that over land. Figure 4f also indicates that less surface evaporation over the ocean is required during the CO_2 ramp-down period for the same precipitation anomaly compared with the CO_2 ramp-up period, because there is less moisture export to land during the CO_2 ramp-down period.

DISCUSSION
The climate system response to changes in the Earth's radiative balance depends on the timescale[48]. The transient climate response, which is formally defined as the global mean surface warming at the time of doubling of CO_2 in an idealized 1% year^{-1} CO_2 increase experiment, quantifies warming in response to a changing forcing prior to the deep ocean being in equilibrium with the forcing. On the other hand, the equilibrium climate sensitivity is defined as the warming for doubling CO_2 in the atmosphere relative to pre-industrial climate, after the climate reached its new equilibrium[49]. To project correctly Earth's future climate, therefore, it is fundamental to understand the transient climate response and equilibrium climate sensitivity[50–52]. In particular, the understanding of the hydrological cycle response to transient climate change is essential for successful adaptation and mitigation policies.

Although the response of the global hydrological cycle has been qualitatively examined by analyzing an atmospheric general circulation model and state-of-the-art climate models, there is little study to examine the contrast of hydrological cycle over land and ocean in a changing CO_2 pathway with large ensemble simulations.

We found that there is an almost linear relationship between precipitation and temperature change for land in response to a changing CO_2 concentration, which contrasts with the asymmetric relationship of precipitation and temperature change over the ocean. Our results indicate that ocean heat uptake and land–ocean warming contrast is the key to the contrasting precipitation responses between land and oceans. The oceans absorb heat until the middle of the CO_2 ramp-down period and it continues to release heat despite a fixed CO_2 concentration during the stabilization period, resulting in an asymmetric relationship of precipitation and temperature changes constrained by surface energy budget. In particular, the CO_2 radiative forcing drives an additional increase in precipitation as land temperatures rise, which could be related to land–ocean temperature contrast. In contrast, ocean precipitation changes from CO_2 radiative forcing are suppressed during the ramp-down period. This result implies that changing CO_2 pathway mitigation and adaptive actions should incorporate the contrasting hydrological cycle responses of the land and ocean, and underlines the importance of confirming simulated responses in the hydrological cycle to CO_2 across all timescale from days to decades. In addition, it would be necessary to examine the hydrological cycle to CO_2 radiative forcing over the tropical vs. the extratropical to understand its regional characteristics.

All analyses used the annual mean of the 28-member ensemble in the present study; however, it would be valuable to understand how the seasonality of precipitation to CO_2 forcing changes over land and the ocean. Transient climate changes and slow adjustment processes during the stabilization period were not found to substantially affect the seasonality of precipitation over both land and ocean, only the magnitude (Supplementary Fig. 6).

Although the ramp-up and ramp-down periods are symmetric in terms of CO_2 concentrations, they are not symmetric at all in terms of forcing relative to the PD climate, as extra heating relative to the PD climate is occurring during both ramp-up and ramp-down periods. The climate system at the beginning of the stabilization period has already absorbed the integrated effects of extra heating during both ramp-up and ramp-down periods. Therefore, the stabilization period is unlike the PD climate in terms of heat content and distribution in the ocean in spite of the same CO_2 concentration. This hysteresis of the global hydrological cycle is expected to be less apparent if assessing in the context of a symmetrical ramp-up and ramp-down in radiative forcing. In that case, there would be no net heat loss or gain after the 280 years relative to the PD climate in which any hysteresis could be weak. Although the present study focuses on the climate transition from CO_2 ramp-up to ramp-down, it would be also necessary to understand the slow adjustment process during the stabilization period.

METHODS
CESM1 experiments
To investigate the hydrological cycles' contrasting response over land and ocean to CO_2 emission ramp-up and ramp-down, we conducted experimental climate model simulations. The model used in this study is a fully coupled CESM1, which has the same component models and coupling of the CESM1 with the Community Atmosphere Model version 5 in CMIP5. CESM1 is the Community Atmosphere Model version 5 coupled to the Parallel Ocean Program version 2, the Community Land Model version 4, and the Los Alamos Sea Ice Model, all at ~1° horizontal

resolution[53]. Vertical resolutions were 30 and 60 levels for the atmosphere and ocean, respectively. The land carbon cycle was also included[54].

We performed two kinds of simulations. One is a PD simulation with a constant CO_2 concentration ($1\times CO_2$, 367 p.p.m.) of over 900 years, where we extracted 28 initial conditions from the PD simulation. The 28 initial ocean condition was taken from the PD simulation arbitrarily. Also, a CO_2 ramp-up and -down experiment was performed in each 28 ensemble member. This experiment employed an increasing atmospheric CO_2 concentration at a rate of 1% year^{-1} until CO_2 quadrupling ($4\times CO_2$, 1478 p.p.m., CO_2 ramp-up simulation) and then a decreasing CO_2 forcing to the same rate over 140 years until reaching the original value ($1\times CO_2$, 367 p.p.m., CO_2 ramp-down simulation). In addition, we integrated a restoring run of 120 years with a constant CO_2 concentration ($1\times CO_2$, 367 p.p.m., CO_2 stabilization simulation).

Simple model for global precipitation response

Global mean precipitation response (ΔP) is balanced by the fast component ($f\Delta F$) in which the atmosphere rapidly adjusts to changes in top of atmosphere radiative forcing, ΔF, and a slow component ($a_{global}\Delta T$), which quantifies the global mean precipitation response to the global mean surface temperature change, ΔT, as follows[2]:

$$\Delta P \sim -f\Delta F + a_{global}\Delta T \qquad (7)$$

where f is the fraction of radiative forcing manifest in the atmosphere and a_{global} is the global hydrological sensitivity that quantifies the global mean precipitation response to the global mean temperature warming alone. It is noteworthy that a_{global} is obtained from the stabilization period in CESM1 experiment (Fig. 2a and Supplementary Fig. 3c, e), 2.54% K^{-1}. f is 0.8 for the fraction of the CO_2 forcing that heats the atmosphere[36]. In addition, the ΔF can be simplified as 5.35ln (CO_2/367 p.p.m.)[55] and ΔT is the model simulated surface temperature response in a CESM. Based on this simple model, we are able to calculate the estimated global mean precipitation response to a CO_2 radiative forcing and compare with the results in CESM1 experiment (Fig. 1d).

Apparent hydrologic sensitivity over land

We define the proportionality constant, κ (i.e., the apparent hydrological sensitivity), as both the fast and slow precipitation response in the ocean and land during the CO_2 ramp-up and ramp-down periods, respectively. However, land's hydrological sensitivity is nearly identical during the ramp-up (↑) period (1.57% K^{-1}) and ramp-down (↓) period (1.61% K^{-1}) (see Fig. 3b), indicating the following relationship:

$$\Delta P_{land} = k_{land}\Delta T_{land}(ramp - up(\uparrow) \text{ and } ramp - down(\downarrow) \text{ periods}) \qquad (8)$$

Here, $\kappa_{land} = (\kappa_{land\uparrow} + \kappa_{land\downarrow})/2$, i.e., 1.59% K^{-1}.

REFERENCES

1. Allan, R. P. & Soden, B. J. Atmospheric warming and the amplification of precipitation extremes. *Science* **321**, 1481–1484 (2008).
2. Allen, M. R. & Ingram, W. J. Constraints on future changes in climate and the hydrologic cycle. *Nature* **419**, 228–232 (2002).
3. Cubasch, U. & Meehl, G. In *Climate Change 2001: The Scientific Basis* (eds. Houghton, J. T. et al.) 525–582 (Cambridge Univ. Press, 2001).
4. Haug, G. H. et al. Climate and the collapse of Maya civilization. *Science* **299**, 1731–1735 (2003).
5. Lemordant, L., Gentine, P., Swann, A. S., Cook, B. I. & Scheff, J. Critical impact of vegetation physiology on the continental hydrologic cycle in response to increasing CO2. *Proc. Natl Acad. Sci. USA* **115**, 4093–4098 (2018).
6. Lesk, C., Rowhani, P. & Ramankutty, N. Influence of extreme weather disasters on global crop production. *Nature* **529**, 84–87 (2016).
7. Ma, J. et al. Hydrological cycle changes under global warming and their effects on multiscale climate variability. *Ann. NY Acad. Sci.* **1472**, 21–48 (2020).
8. Roderick, M., Sun, F., Lim, W. H. & Farquhar, G. A general framework for understanding the response of the water cycle to global warming over land and ocean. *Hydrol. Earth Syst. Sci.* **18**, 1575–1589 (2014).
9. Schiermeier, Q. Increased flood risk linked to global warming. *Nature* **470**, 316 (2011).
10. Coumou, D. & Rahmstorf, S. A decade of weather extremes. *Nat. Clim. Change* **2**, 491–496 (2012).
11. Diffenbaugh, N. S. et al. Quantifying the influence of global warming on unprecedented extreme climate events. *Proc. Natl Acad. Sci. USA* **114**, 4881–4886 (2017).
12. Peterson, T. C., Stott, P. A. & Herring, S. Explaining extreme events of 2011 from a climate perspective. *Bull. Am. Meteorol. Soc.* **93**, 1041–1067 (2012).
13. Arnell, N. W., Lowe, J. A., Challinor, A. J. & Osborn, T. J. Global and regional impacts of climate change at different levels of global temperature increase. *Clim. Change* **155**, 377–391 (2019).
14. Arnell, N. W. et al. The global and regional impacts of climate change under representative concentration pathway forcings and shared socioeconomic pathway socioeconomic scenarios. *Environ. Res. Lett.* **14**, 084046 (2019).
15. Watts, N. et al. Health and climate change: policy responses to protect public health. *Lancet* **386**, 1861–1914 (2015).
16. Kundzewicz, Z. W. et al. Flood risk and climate change: global and regional perspectives. *Hydrol. Sci. J.* **59**, 1–28 (2014).
17. Collins, M. et al. In *Climate Change 2013: The Physical Science Basis* (eds. Stocker, T. F. et al.) 1029–1136 (Cambridge Univ. Press, 2013).
18. Held, I. M. & Soden, B. J. Robust responses of the hydrological cycle to global warming. *J. Clim.* **19**, 5686–5699 (2006).
19. Chou, C., Neelin, J. D., Tu, J.-Y. & Chen, C.-T. Regional tropical precipitation change mechanisms in ECHAM4/OPYC3 under global warming. *J. Clim.* **19**, 4207–4223 (2006).
20. Chou, C., Neelin, J. D., Chen, C.-A. & Tu, J.-Y. Evaluating the "rich-get-richer" mechanism in tropical precipitation change under global warming. *J. Clim.* **22**, 1982–2005 (2009).
21. Xie, S.-P. et al. Global warming pattern formation: sea surface temperature and rainfall. *J. Clim.* **23**, 966–986 (2010).
22. Huang, P., Xie, S.-P., Hu, K., Huang, G. & Huang, R. Patterns of the seasonal response of tropical rainfall to global warming. *Nat. Geosci.* **6**, 357–361 (2013).
23. Chou, C. & Chen, C.-A. Depth of convection and the weakening of tropical circulation in global warming. *J. Clim.* **23**, 3019–3030 (2010).
24. Allan, R. P. et al. Advances in understanding large-scale responses of the water cycle to climate change. *Ann. NY Acad. Sci.* **1472**, 49–75 (2020).
25. Wu, P., Ridley, J., Pardaens, A., Levine, R. & Lowe, J. The reversibility of CO2 induced climate change. *Clim. Dyn.* **45**, 745–754 (2015).
26. Cao, L., Bala, G. & Caldeira, K. Why is there a short-term increase in global precipitation in response to diminished CO2 forcing? *Geophys. Res. Lett.* **38**, https://doi.org/10.1029/2011GL046713 (2011).
27. Boucher, O. et al. Reversibility in an Earth System model in response to CO2 concentration changes. *Environ. Res. Lett.* **7**, 024013 (2012).
28. Keller, D. P., Feng, E. Y. & Oschlies, A. Potential climate engineering effectiveness and side effects during a high carbon dioxide-emission scenario. *Nat. Commun.* **5**, 3304 (2014).
29. Ricke, K. L. & Caldeira, K. Maximum warming occurs about one decade after a carbon dioxide emission. *Environ. Res. Lett.* **9**, 124002 (2014).
30. Mitchell, T. D. Pattern scaling: an examination of the accuracy of the technique for describing future climates. *Clim. Change* **60**, 217–242 (2003).
31. Wilby, R. L. et al. A review of climate risk information for adaptation and development planning. *Int. J. Clim.* **29**, 1193–1215 (2009).
32. McNutt, M. K. et al. *Climate Intervention: Carbon Dioxide Removal and Reliable Sequestration* (National Research Council of the National Academies, 2015).
33. Chadwick, R., Wu, P., Good, P. & Andrews, T. Asymmetries in tropical rainfall and circulation patterns in idealised CO2 removal experiments. *Clim. Dyn.* **40**, 295–316 (2013).
34. Andrews, T. & Forster, P. M. The transient response of global-mean precipitation to increasing carbon dioxide levels. *Environ. Res. Lett.* **5**, 025212 (2010).
35. Samanta, A. et al. Physical climate response to a reduction of anthropogenic climate forcing. *Earth Interact.* **14**, 1–11 (2010).
36. Andrews, T., Forster, P. M., Boucher, O., Bellouin, N. & Jones, A. Precipitation, radiative forcing and global temperature change. *Geophys. Res. Lett.* **37**, L14701 (2010).

37. Wu, P., Wood, R., Ridley, J. & Lowe, J. Temporary acceleration of the hydrological cycle in response to a CO2 rampdown. *Geophys. Res. Lett.* **37**, L12705 (2010).
38. Samset, B. H. et al. Weak hydrological sensitivity to temperature change over land, independent of climate forcing. *npj Clim. Atmos. Sci.* **1**, 1–8 (2018).
39. Richardson, T. et al. Drivers of precipitation change: an energetic understanding. *J. Clim.* **31**, 9641–9657 (2018).
40. Tebaldi, C. & Knutti, R. The use of the multi-model ensemble in probabilistic climate projections. *Philos. Tran. R. Soc.* **365**, 2053–2075 (2007).
41. Deser, C., Phillips, A., Bourdette, V. & Teng, H. Uncertainty in climate change projections: the role of internal variability. *Clim. Dyn.* **38**, 527–546 (2012).
42. Allan, R. P. et al. Physically consistent responses of the global atmospheric hydrological cycle in models and observations. *Surv. Geophys.* **35**, 533–552 (2014).
43. Boer, G. Climate change and the regulation of the surface moisture and energy budgets. *Clim. Dyn.* **8**, 225–239 (1993).
44. Lambert, F. H. & Webb, M. J. Dependency of global mean precipitation on surface temperature. *Geophys. Res. Lett.* **35**, L16706 (2008).
45. Berg, P., Moseley, C. & Haerter, J. O. Strong increase in convective precipitation in response to higher temperatures. *Nat. Geosci.* **6**, 181–185 (2013).
46. Byrne, M. P. & O'Gorman, P. A. The response of precipitation minus evapo-transpiration to climate warming: Why the "wet-get-wetter, dry-get-drier" scaling does not hold over land. *J. Clim.* **28**, 8078–8092 (2015).
47. Nuijens, L. & Siebesma, A. P. Boundary layer clouds and convection over sub-tropical oceans in our current and in a warmer climate. *Curr. Clim. Change Rep.* **5**, 80–94 (2019).
48. Knutti, R., Rugenstein, M. A. & Hegerl, G. C. Beyond equilibrium climate sensitivity. *Nat. Geosci.* **10**, 727–736 (2017).
49. Randall, D. A. et al. In *Climate Change 2007: The Physical Science Basis* (eds. Solomon, S. et al.) 589–662 (Cambridge Univ. Press, 2007).
50. Knutti, R., Stocker, T. F., Joos, F. & Plattner, G.-K. Constraints on radiative forcing and future climate change from observations and climate model ensembles. *Nature* **416**, 719–723 (2002).
51. Hegerl, G. C. et al. In *Climate Change 2007: The Physical Science Basis* (eds. Solomon, S. et al.) 663–746 (Cambridge Univ. Press, 2007).
52. Meehl, G. A. et al. In *Climate Change 2007: The Physical Science Basis* (eds. Solomon, S. et al.) 747–845 (Cambridge Univ. Press, 2007).
53. Hurrell, J. W. et al. The community earth system model: a framework for collaborative research. *Bull. Am. Meteorol. Soc.* **94**, 1339–1360 (2013).
54. Lawrence, D. M. et al. Parameterization improvements and functional and structural advances in version 4 of the Community Land Model. *J. Adv. Model. Earth Syst.* **3**, M03001 (2011).
55. Myhre, G., Highwood, E. J., Shine, K. P. & Stordal, F. New estimates of radiative forcing due to well mixed greenhouse gases. *Geophys. Res. Lett.* **25**, 2715–2718 (1998).

COMPETING INTERESTS
The authors declare no competing interests

ADDITIONAL INFORMATION
Supplementary information The online version contains supplementary material available at https://doi.org/10.1038/s41612-021-00206-6.

Correspondence and requests for materials should be addressed to Sang-Wook Yeh.

Reprints and permission information is available at http://www.nature.com/reprints

Publisher's note Springer Nature remains neutral with regard to jurisdictional claims in published maps and institutional affiliations.